Optimized Position Sensors for Flying-Spot Active Triangulation Systems

Beraldin, Jean-Angelo; Blais, François; Rioux, Marc; Domey, Jacques; Gonzo, L.; De Nisi, F.; Comper, F.; Stoppa, D.; Gottardi, M.; Simoni, A.

National Research Council Canada
Conseil national de recherches Canada

Institute for Information Technology
Institut de technologie de l'information

NRC · CNRC

Optimized Position Sensors for Flying-Spot Active Triangulation Systems *

Beraldin, J.-A., Blais, F., Rioux, M., Domey, J., Gonzo, L., De Nisi, F., Comper, F., Stoppa, D., Gottardi, M. Simoni, A.
October 2003

* published in Proceedings of the Fourth International Conference on 3-D Digital Imaging and Modeling (3DIM). Banff, Alberta, Canada. October 6-10, 2003. pp 334-341. NRC 47083.

Canada

Optimized Position Sensors for Flying-Spot Active Triangulation Systems

J-A Beraldin, F. Blais, M.Rioux, J. Domey
National Research Council of Canada,
Ottawa, Canada, K1A 0R6
angelo.beraldin@nrc-cnrc.gc.ca

L. Gonzo, F. De Nisi, F. Comper, D. Stoppa, M. Gottardi and A. Simoni
ITC-irst Centre for Scientific and Technological Research
I-38050 Povo, Trento, Italia
lgonzo@itc.it

Abstract

A description of the integrated sensors developed for flying-spot active triangulation will be given. All the sensors have been fabricated using standard CMOS technology that allows the monolithic integration of photo-sensors, together with readout circuits, and digital signal processors. Position sensors are classified into two classes that allow a better understanding of the pros and cons of each one. A description of the proposed position sensor that is optimized for accurate and fast 3D acquisition is given alongside some experimental results.

1. Introduction

Digital 3D imaging can benefit from advances in VLSI technology in order to accelerate its deployment in many fields like visual communication, heritage and industrial automation. Like many other technologies before, miniaturizing has made possible systems with increased performance, accessibility, and, lower maintenance, size and cost. Monolithic integration of photo-sensors, together with readout circuits, and digital signal processors are described in this paper in the context of flying-spot active triangulation [1]. The position sensors (PS) proposed here will become an integral part of our future intelligent digitizers that will be capable of measuring accurately and at high data rate registered color (reflectance) and 3D coordinates. This, in turns, will accelerate the development of multi-resolution hand-held 3D cameras with fast search/track capabilities [2-3]. VLSI integration of the range detection functions will be required to achieve the benefits of miniaturization.

Section 2 gives a brief description of the different methods available for digital 3D imaging. Laser-based triangulation is described in more details along with the requirements that are specific to these cameras. Section 3 presents the state of the art in laser spot position sensing methods by dividing them in two broad classes according to the way the spot position is sensed. These are categorized as Continuous Response Position Sensors (CRPS) and Discrete Response Position Sensors (DRPS). Section 4 presents the two sensors targeted for integration onto VLSI CMOS, i.e., Colorange and ColorSense. Implementation details and experimental results for the proposed sensors optimized for digital 3D imaging are presented in section 5. Finally, concluding remarks appear in section 6.

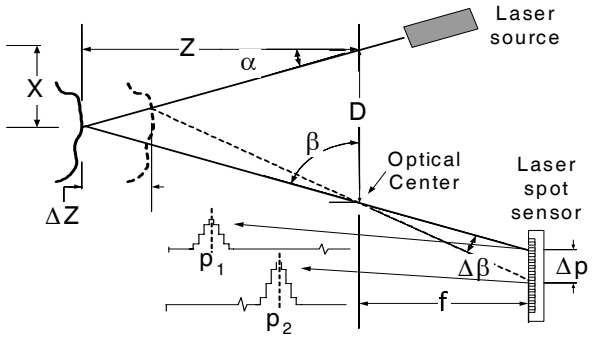

Figure 1. Laser-based optical triangulation

2. Requirements for laser-based systems

To recover the geometrical structure of visible surfaces of objects that are rather featureless to the human eye or a video camera, people have resorted to active vision. Active vision attempts to reduce the ambiguity of scene analysis by structuring the illumination onto a scene. Thus, the task of generating 3D coordinates is greatly simplified. Moreover, with laser-based approaches, the 3D information becomes relatively insensitive to background illumination, surface texture and large depth of fields can be achieved. Lidar-based and triangulation-based laser range cameras are examples of vision systems built around such strategy [4]. Some range cameras provide registered range and intensity data (either monochrome or color) [5].

Figure 1 depicts the optical geometry of an optical probe (single 3D point) based on triangulation. In order to capture a 3D surface map, a laser spot is scanned onto a scene by way of accurate deflecting mirrors [3,10-11].

The basic laser probe will be used in the following calculations. The collection of the scattered laser light from the surface is done at a different vantage point (triangulation). This light is focused onto a position sensitive detector (herein called position sensor). The laser beam can be of a single wavelength (visible or infrared) or composed of multiple visible wavelengths for the purpose of measuring the color map of a scene (reflectance map).

One can relate the geometry found in this optical probe with the law of cosines. Knowing two angles (α and β) of a triangle relative to its base (baseline **D**) determines the dimensions of this triangle. By simple trigonometry, the **(X,Z)** coordinate of the illuminated point on the object is

$$Z = \frac{D\,f}{p + f\,\tan(\alpha)} \qquad \textbf{(1)}$$

$$X = Z\,\tan(\alpha) \qquad \textbf{(2)}$$

where **p** is the position of the imaged spot on the position sensor (PS), α is the deflection angle (or fixed angle) of the laser beam, **D** is the separation between the lens and the laser source (camera baseline), and **f** is the effective distance between the position sensor and the lens. This can be restated as follows. For an incremental change of distance, Δ**Z**, one measures the incremental angle shift $\Delta\beta$ using the theorem of opposite angles. The PS is in fact an *angle sensor*. The angular shift $\Delta\beta$ caused by the displacement of the surface is observed through a shift in laser spot position $\Delta p=(p_1 - p_2)$. For practical matters, the errors come mainly from the estimate of **p**, through σ_p. Applying the propagation of errors to equation (1) gives the approximation of the standard deviation

$$\sigma_z \approx \frac{Z^2}{f\,D}\sigma_p \qquad \textbf{(3)}$$

where σ_z is the standard deviation of the error in the measurement of **Z** (representative of the measurement uncertainty), which is inversely proportional to both the camera baseline and the effective focal length of the lens, but directly proportional to the square of the distance. Other forms of equations (1), (2) and (3) exist. They relate **z** uncertainty to triangulation angle and numerical aperture of the laser projector.

The value of σ_p depends on the type of PS used, the limitations of commercial devices and on the physical limits of laser-based 3D active vision systems. People in high-energy physics have been using PS for years. Detectors like position-sensitive photomultiplier tubes PMT (or micro-channel plates MCP), gas amplifier detectors, and micro-strip solid-state detectors are customary in that field. Though interesting, these are not appropriate and cost effective for laser scanners. We are interested in monolithic PS like photodiode arrays, CCD arrays and lateral effect photodiodes that are based on commercial silicon technology. In particular, we want to design optimized PS. That because, commercial photodiode arrays or CCD used in 3D vision sensors are intended for 2D imaging applications, spectroscopic instruments or wavelength division multiplexing in telecommunication systems. Their specifications change according to the evolution of their respective fields and not to digital 3D imaging. For instance, speckle noise found in laser-based systems dictates a large pixel size [6,11] that is not compatible with current 2D imaging sensors (where the pixel size is in the order of 4 to 5 μm). These considerations are the basis for investigating PSs optimized for laser-based 3D imaging.

The following section presents a summary of the PSs used for laser spot position measurement that have been published in recent years. The other sections present our solution to attain high 3D data throughputs, high accuracy and low measurement uncertainty.

3. Laser position sensors for triangulation

Many devices have been built in the past and in recent years for measuring the position of a light beam. Among those, one finds Continuous Response Position Sensors

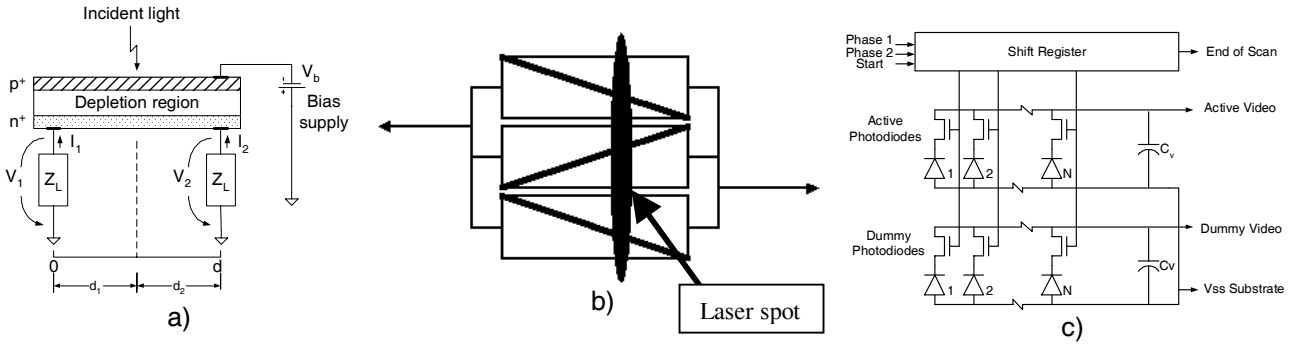

Figure 2. Schematic diagram of some PS: a) CRPS-LEP, b) CRPS-wedged LEP, c) DRPS- MPXA

(CRPS) and Discrete Response Position Sensors (DRPS). The category CRPS includes lateral effect photodiode **LEP** (see Figure 2a) and geometrically shaped photodiodes (wedges – Figure 2b or segmented). DRPS on the other hand comprise detectors such as Charge Coupled Devices (CCD) and arrays (1-D or 2-D) of photodiodes equipped with a multiplexer (MPXA) for sequential reading like the one schematically represented on Figure 2c. Other types exist but are not shown here. The references included in this paper provide detailed information about this topic [7,11,13-14].

3.1. Continuous response PS

A CRPS provides the centroid of the light distribution impinging on its surface [7-11]. The response time can be very fast, i.e. in the order of 10 MHz [10]. The spot position uncertainty, σ_p, can be expressed in terms of speckle noise and thermal noise components. Baribeau and Rioux [6] predict (when the collected signal amplitude is high wrt thermal/shot noise) that speckle noise for a centroid detector behaves like a Gaussian process and that the estimated rms fluctuation σ_{pS} of **p** determined by such noise is given by

$$\sigma_{pS} = \frac{\lambda f}{\pi \sqrt{2}\ \Theta \cos(\tau)} \qquad \textbf{(4)}$$

where λ is the wavelength of the laser source, f is the effective position of the imaging lens, Θ is the lens diameter, and τ is the tilt angle of the position sensor [6]. The thermal noise has also an effect on the spot position uncertainty especially at high data rates above 50 kHz and when lateral effect photodiodes (LEP) are used [8-9,11]. This uncertainty is approximately given by

$$\sigma_{pT} \approx L \frac{\sqrt{\frac{4kTB}{R}}}{P_s \Re_\lambda} \qquad \textbf{(5)}$$

where $\Re_\lambda$ is the responsivity at a given wavelength λ, T the operating temperature, k is Boltzmann's constant, P_s is the laser power impinging on the LEP, L the length of the sensor, B is the system bandwidth, and R is the inter-electrode resistance. Please note the explicit dependence of σ_{pT} with the collected signal amplitude. These two noise sources can be added directly in quadrature because they are uncorrelated. Detailed calculations of the total electronic noise component as a function of frequency and type of noise are given ref. [9]. In a typical high-speed (>50kHz), laser-based triangulation system that uses a LEP, thermal noise will limit the detection process (σ_z) and not speckle noise. In the case of other popular PS used in centering applications, e.g. Bi-cells or Quad-cells, linearity is traded for speed and lower noise [8]. Hence, speckle noise has to be considered in the system error budget.

To complete the analysis, one must mention that what limits CRPS is the fact that the shape of the distribution of light on the surface of the sensor is never known but always assumed symmetrical. Spurious light cannot be separated from the actual spot position information and is interpreted as valid information. The resulting spot position estimate will be erroneous. The following section discusses this topic and presents a PS that can cope with spurious light.

3.2. Discrete response PS

Sensors that provide the information about the shape of the light distribution impinging on the sensor are categorized as DRPS. The word *Discrete* is used in the sense that the distribution (that is continuous) is provided in a sampled version. For instance, CCD arrays and photodiodes arrays are classified as a DRPS. What characterizes this class of sensors is that when combined with appropriate signal processing algorithms, it becomes possible to eliminate false measurements generated by a cluttered environment from those measurements that truly represent a selected point on the target surface.

Table 1 lists the most important sources of noise and interference sources present in the digitized signal. Some of the sources of noise listed have a multiplicative effect on the signal (e.g. laser speckle and object reflectivity), others are purely additive (e.g., electrical noise, external illumination), or introduce distortions in the signal (e.g., aliasing, focusing, jitter).

Although some of these sources of interference can be reduced by proper design, they cannot be totally eliminated. For example, an optical interference filter will reduce the optical effects of the sun and ambient illumination, but it won't eliminate them. This is shown in Figure 3 where an optical interference filter was used but was unable to remove the direct sunlight. When

Table 1. Sources of noise and interference

External illumination	Ambient illumination, Direct sunlight interference, Other lasers
Laser	Laser speckle, Laser focusing, Laser power, Object reflectivity
Electrical	Electromagnetic interference, clock-induced noise & clock harmonics, reset noise, thermal and shot noise
Other	Signal jitter (e.g. video sync.), Quantification (A-D conversion), Image aliasing, Sensor nonlinearity

considering that situation, a CRPS would provide **A** as an answer. But a DRPS with appropriate signal processing can provide **B**, the desired response (see Figure 3). This situation occurs frequently in real applications. The elimination of all stray light in an optical system requires sophisticated techniques that increase the cost of a system.

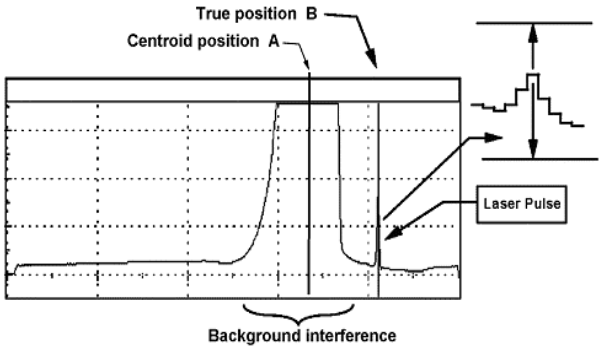

Figure 3. A typical situation where stray light blurs the measurement of the real but much narrower peak. A CRPS would provide A as an answer. But a DRPS can provide B, the desired response peak.

Detection of the laser peak position consists in measuring the position and intensity with maximum accuracy, i.e., to within a fraction of a pixel. The peak position operator that we use is based on a Finite Impulse Response (FIR) derivative filter. It extracts the location of the spot to 1/64th of a pixel, validates the measurements and filters out clock interference and low frequency noise. This filter topology has proven to be quite robust and accurate. A comparison between this technique and other popular techniques such as centroid calculations, single or double thresholding, Gaussian filtering, etc., has been discussed in [13,14]. Baribeau and Rioux [6] approximated, for this type of peak detection operator, the rms fluctuation of **p** determined by speckle noise. It behaves like a Gaussian process and is given by

$$\sigma_p = \frac{\lambda f}{\sqrt{2\pi}\ \Theta\ \cos(\tau)} \qquad \textbf{(6)}$$

According to this equation and assuming again signal amplitude high wrt non-speckle noise sources, $\boldsymbol{\sigma_p}$ for a centroid detector is $\sqrt{\pi}$ better than the one based on a FIR derivative filter (see eqn. 4). But as discussed previously, thermal noise has a greater effect on centroid-based PS than speckle noise and consequently accuracy is not maintained when interference signals are present (like those created by stray light). DRPS, though very accurate, are slower than CRPS because all the photo-detectors have to be read sequentially prior to the measurement of the location of the real peak of the light distribution [13-14]. Commercial DRPS sensors now incorporate window reading or **region-of-interest** (ROI) processing but have been designed for 2D imaging and they don't provide the mechanism to speed-up 3D image acquisition. The following section describes what has been proposed in the literature and presents our approach.

4. Custom PS based on hybrid solutions

One cannot achieve high measurement speed like found with continuous response position sensor and keep the same accuracy as with discrete response position sensors. Mäkynen et al. propose a tracking position sensor that combines the best properties of the conventional lateral effect photodiodes and four-quadrant position sensor [8]. Nezuka et al. [12] propose another interesting PS. Their sensor implements a quad-tree structure to speed-up reading of the photo-sensors after having been thresholded to a binary value. Ando and Kimachi in ref. [18] describe a correlation image sensor to compute the individual angle of a sheet of light at each pixel on the CMOS sensor. Image resolution is still an issue and work is being done to address it. Recently, Massari et al. [16] proposed a DRPS that outputs the centroid of a light distribution. Although the sensor relies on a DRPS it works like a CRPS owing for high readout speed and spot size recovery. A company in Sweden, Integrated Vision Products, designed a single chip CMOS DRPS for high-speed 3D inspection. The sensor is a 2D array of photodiodes and is used in sheet of light 3D range cameras. The chip implements also a DSP which helps in the extraction of the profile from the 2D image collected. These position sensors and others [19-20] are good examples of optimized CRPS or DRPS. Unfortunately, the pixel fill factor is low (high systematic errors [21-22]) and they don't give explicit access to the actual distribution of the laser spot for further processing. To illustrate the importance of knowing the spot distribution, Godin et al. have found that measurement of a marble surface causes increased uncertainty [15]. Furthermore, a bias appears in the depth estimation. Spot shape on the PS changes when measuring a translucent surface like marble. Therefore, analysis of the spot shape can be used to understand and correct this kind of behavior.

As presented in ref. [8,12], we also propose to use the best of both worlds. Theory predicts that a CRPS achieves centroid measurement with a lower uncertainty and high speed with respect to a DRPS. In practice,

measurement uncertainty is important but accuracy is even more important. A CRPS is in fact a *good estimator* of the central location of a light distribution. DRPS are very *accurate* (because of the knowledge of the distribution). In fact, what is required for the measurement of the light distribution peak is only a small portion of the DRPS, i.e., a Region of Interest - ROI. Once the pertinent light distribution is available, one can compute the location of the desired peak very accurately and study the shape of the spot distribution in order to correct any anomalies due to surface reflections. The predicted data rate for this type of sensor is listed in Table 2 according to the ROI size. The assumptions are that the number of samples per scan line is 4096 (close to the diffraction limit [11]) and that the clock rate is 4 MHz (well within CMOS technology). The following section presents two custom PS that we have designed and tested.

Table 2. Predicted system performance according to window size (ROI)

ROI size (pixels)	3D data rate(1)	Laser scanner line rate(2)
16	250 kHz	61 Hz
32	125 kHz	30.5 Hz
64	62.5 kHz	15.26 Hz
128	31.25 kHz	7.63 Hz
256	15.625 kHz	3.81 Hz
512	7.81 kHz	1.91 Hz

(1): Clock rate 4 MHz
(2): 4096-3D points per scan line

4.1. *Colorange* sensor

Let us start with an object that is illuminated by a collimated RGB laser beam (similar to the situation depicted on Figure 1). A portion of the reflected radiation upon entering the system is split into four components by a diffracting optical element (DOE). According to the schematic diagram on Figure 4, the white, zero order component, is aimed at the DRPS, while the RGB 1st order components are projected onto three separate CRPS. These CRPS are used to find an estimate of the centroid of the light distribution impinging on them and to estimate the total light intensity, i.e. for color detection. The centroid ($\mathbf{p_b}$, $\mathbf{p_g}$, $\mathbf{p_b}$) is computed on chip with the well-known current ratio method as described in [9]. The centroid values are fed to a processing element that computes a weighed average of the three centroids, one for each color. The weights are simply a function of the signals variance as per eqn. (5). Then, a control unit selects a **ROI** or window, i.e., a sub-set of contiguous

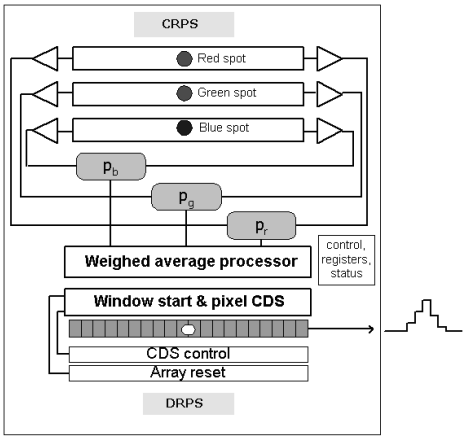

Figure 4. Schematic diagram of the *Colorange* sensor

photo-detectors on the DRPS. That **ROI** is located around the estimate of the centroid supplied by the CRPS. After that, the best algorithm for peak extraction can be applied to the light distribution of interest to find the spot location with sub-pixel accuracy [13-14]. Finally, that value is combined with the location of the **ROI** in order to find the final result.

In a monochrome range camera, a portion of the reflected radiation upon entering the system is split into two beams. One portion is aimed at a single CRPS that determines the location of the best window (**ROI**) and sends that information to the DRPS. The rest of the processing is the same as per the RGB case. In terms of bandwidth requirements, the CRPS will need to be about five times the data rate. For instance, with a **ROI** of 16 pixels, the 3D data rate is 125 kHz and the CRPD must have a signal bandwidth of at least 625 kHz (could be a problem with CMOS – see section 5 on experiments). One should note that the current ratio to compute ($\mathbf{p_b}$, $\mathbf{p_g}$, $\mathbf{p_b}$) needs a resolution of only 4 to 5 bits. The derivation is not given here but can be found in [9].

4.2. *ColorSens* sensor

Here we propose the use of two DRPS, integrated on the same chip or on the same package. The sensor is illustrated on Figure 5. The two sensors work in storage mode and process the light distribution simultaneously.

The incoming light beam might either be split into two components, each aimed at one DRPS, or can be properly shaped for striking both DRPS. The DRPSs are designed to have 2^n and 2^k pixels, respectively, with n<k. Possible values for n and k could be 5 and 8 respectively. The first DRPS, hereafter DRPS_A, is used to calculate a raw estimate of the spot position, while the second DRPS, hereafter DRPS_B, is used to calculate the spot

position with higher accuracy on the base of information passed by DRPS_A. This latter has bigger pixels than DRPS_B and therefore needs a lower integration time for producing a manageable signal. The photo-generated signal from each pixel of DRPS_A is fed into a winner-take-all circuit (**WTA**), as shown in Figure 6, where the decision on what pixel has produced the largest photo-signal is taken.

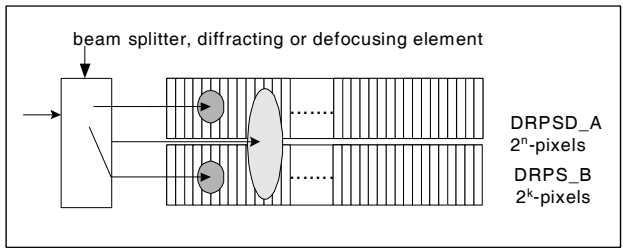

Figure 5. Illustration of the *ColorSense*

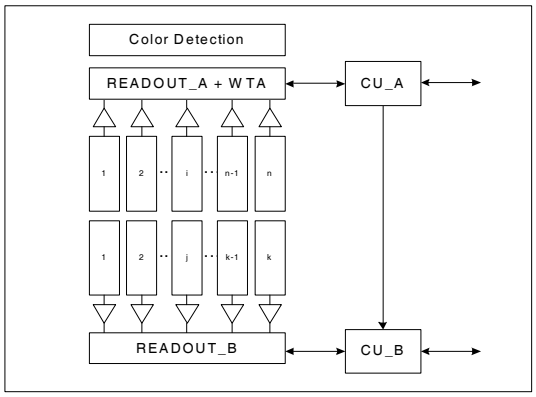

Figure 6. Block diagram of the electronic detection circuitry

The working principle of the WTA can be summarized as follows: the output of each pixel in DRPS_A is compared with a voltage ramp generated by proper circuitry. The output with highest voltage value intercepts the ramp first and inhibits the functionality of all other comparators by means of a logical feedback network. The WTA exhibits therefore at the output the coordinate of the pixel, which has received the largest amount of light. This information is further processed by control unit CU_A which calculates the address of a sub-window of say 2^m pixels (m<k, typical values might be m = 4 or 5), on DRPS_B, centered on the raw spot position given by DRPS_A. DRPS_B has a higher pixel resolution and is therefore suited for the accurate spot position detection. Only the pixels addressed by the sub-window are read out for a greatly increased 3D measurement rate. Here too, the best algorithms for peak extraction can be applied to the light distribution of interest [13-14]. We assume that because the incoming beam is split into two beams, the system can compensate by doubling the laser power of the source.

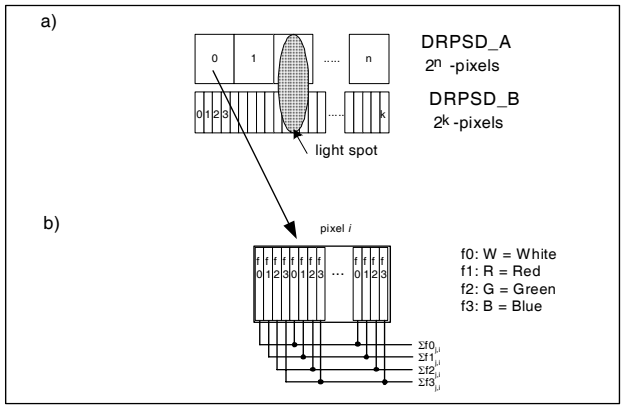

Figure 7. One possible pixel geometry for spot and color detection

Slight modification of this architecture can also be used for color detection, as shown in Figure 7a and Figure 7b. Here each single pixel of DRPS_A is further divided into elementary photocells f_i, i = 0 to r, each one covered with an appropriate optical filter. In Figure 7b, r=3 and the filters can for example be of type R, G and B; Uncovered or W elementary cell (of type f0 in Figure 7b) must be preserved for the raw spot position detection. The number of elementary cells is limited only by the photolithography of the filters. All of these elementary cells, within the same pixel, carrying the same filter as well as the uncovered cells are connected in parallel to a readout channel as shown in Figure 7b which gives both the raw spot position and R, G, B and W intensities. The geometry of the elementary pixels might be as those shown in Figure 7b or be of other kind (squared pixels, for example), provided that roughly the same number of elementary cells for each color and for the uncovered cells are illuminated.

The use of two DRPS differing only for the pixels geometries makes them suitable for integration on the same chip using the same process. This reduces greatly

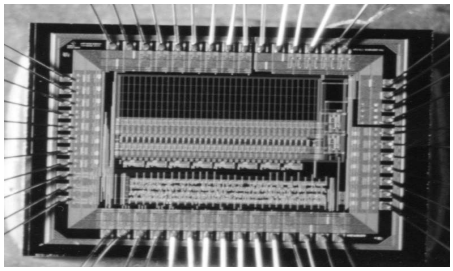

Figure 8. Die photograph of part of the *Colorange* sensor

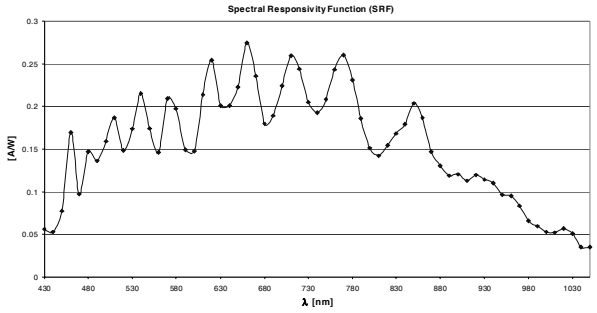

Figure 9. Spectral responsivity of p-n photodiodes fabricated in 0.8 μm CMOS

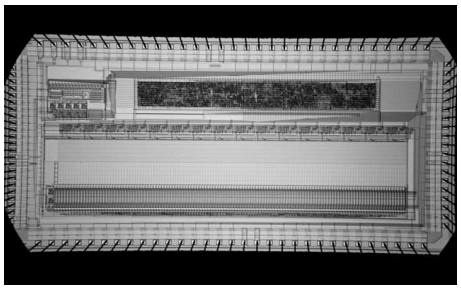

Figure 10. Die photograph of the ColorSens chip

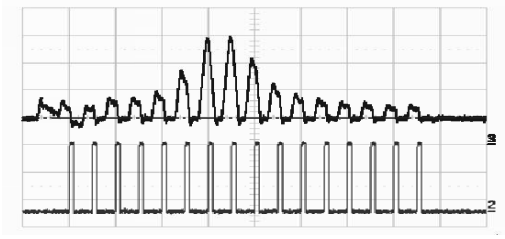

Figure 11. Spot intensity and size recovery from DRPS_B in ColorSens

production and alignment costs. Furthermore, filter deposition is accomplished as a post-processing step. It is carried out either within the same fabrication foundry who produced the chip or by a third party. Although, simple optics can be used for beam splitting or shaping, the use of μ-lenses as a post-processing step is being investigated.

5. Experimental results

Prototypes of the two type of sensors presented in Section 4 have been implemented in standard CMOS technology using 0.8μm and 0.6μm processes for the *Colorange* and *ColorSens*, respectively. Both devices have been designed according to some basic electro-optical specifications like the minimum and maximum spot intensity on the sensor which typically covers three orders of magnitude with minimum values in the nW range, spot diameter ranging between 200μm and 600μm, readout speed in the range of 50 kHz (100 kHz for next generation sensors), and dynamic range better than 12 bits. A summary of the experimental results is given below.

The *Colorange* device (CR), shown in Figure 8, contains a single array of 32 pixels with a 50μm pitch. Each pixel is composed by a photodiode PD, and a readout channel with noise suppressing correlated double sampling (CDS) circuitry. The working principle of the pixel is that typical for many imaging sensors, i.e. storage mode. This means that the photodiode is first biased to a reset voltage and then left floating to integrate the light. Finally, after the integration time, the accumulated charge is transferred to the readout circuit, properly filtered and sent to the output interface. The photodiode is a $500\times48\mu m^2$ n-p junction and its measured spectral responsivity is shown in Figure 9.

The integration of the CRPS presently has been done on a different chip and experimental tests are being undertaken. However, in light of these preliminary experimentations, some considerations can be done regarding the performance that can be expected. The main consideration regards the fabricating process: most CMOS processes in fact are not yet optimized for optical sensors. Therefore a CMOS-CRPS will have a much lower resistance and a much higher capacitance with respect to those fabricated with proprietary processes [8]. This leads basically to two detrimental effects: first the device will be slower and noisier and second, ghost effect will appear due to the diffusing charges generated within the substrate [17]. Similar effects are present with segmented (wedge-shaped) lateral effect photodiodes.

The ColorSens type device (CS) is the practical evolution of the CR, as it results from the attempt of increasing the performances of the latter. The die photograph of the device is shown in Figure 10. The two arrays of pixels are butted on top of each other along their major side. DRPS_A, responsible for the raw position and intensity estimation, is composed of 16 pixels (n=4) each one $400\times1100\mu m^2$ in size. As for the *Colorange*, each pixel consists in a photodiode and a variable gain readout channel. The photodiode measures $400\times500\mu m^2$ and is divided into 5 groups of R,G,B and W photodiodes for color detection as explained in section 4.2. DRPS_B, which is used for the accurate measurement of the spot position as well as its shape, is composed of 128 pixels (k=7) each measuring 50×1000

μm^2. Here the photodiode area is $48 \times 500\ \mu m^2$. The pixel fill factor is close to 96% (which is much higher than [12,19-20]). Gain selection, for the charge amplifier, are set by the internal processing unit which calculates the right gain value on the basis of the total intensity as read from W channels. Spectral as well as power responsivity of the CS pixels are very similar to those reported for the *colorange* sensor. For this chip, the value of m, defined in section 4.2 is equal to 4 so only 16 pixels out of the 128 are considered for the accurate spot position determination. Figure 11 shows the output when the spot is centered on one of the DRPS_A pixels. A more critical situation occurs when the spot falls right in between two DRPS_A pixels. In both cases. the spot position can be recovered with the proper accuracy. Other outputs of the device are of course: the coordinate of the raw position, the intensity on the R, G, B and W channels as well as flags indicating the number of W channels which have crossed the minimum signal threshold.

6. Conclusions

The results obtained so far have shown that optical sensors have reached a high level of development and reliability that are suited for high accuracy 3D vision systems. The availability of standard fabrication technologies and the acquired know-how in the design techniques, allow the implementation of optical sensors that are application specific: Opto-ASICs. The trend shows that the use of the low cost CMOS technology leads competitive optical sensors. Furthermore, post-processing modules, as for example anti-reflecting coating film deposition and RGB filter deposition to enhance sensitivity and for color sensing, are at the final certification stage and will soon be available in standard fabrication technologies. Integration of most low level processing steps on a chip using advances in VLSI CMOS will allow digital 3D imaging technology to become widely accepted and accessible to universities, research labs, industries, hobbyists, and, maybe to the home.

7. References

[1] M. Rioux, "Laser Range Finder based on Synchronized Scanners," Appl. Opt., 23, 1984, pp. 3837-3844.

[2] Hébert, P. and Rioux, M., "Toward a hand-held laser range scanner: integrating observation-based motion compensation," SPIE's 10th Intern. Symp. Elec. Imaging, Jan. 1998, pp. 24-30.

[3] Blais, F., Picard, and M. Godin, G. "Recursive Model Optimization Using ICP and Free Moving 3D Data Acquisition," Proc. of 4th Intern. Conf. on 3-D Digital Imaging and Modeling (3DIM2003), Oct. 6-10, 2003, Banff, Canada.

[4] P.J. Besl, "Range Imaging Sensors," Machine Vision and Applications (1), 1988, pp. 127-152.

[5] R. Baribeau, M. Rioux, and G. Godin. "Color reflectance modeling using a polychromatic laser range sensor," IEEE Trans. Pattern Anal. Mach. Intell. 14(2), 1991, pp. 263-269.

[6] R. Baribeau, and M. Rioux, "Influence of Speckle on Laser Range Finders," Appl. Opt., 30, 1991, pp. 2873-2878.

[7] L. Gonzo, A. Simoni, M. Gottardi, D. Stoppa and J-A Beraldin, "Sensors Optimized for 3D Dititization," IEEE Trans. on Instr. and Meas., In Press.

[8] A. Makynen, T. Ruotsalainen, T. Rahkonen, J. Kostamovaara, "High performance CMOS position-sensitive photodetectors (PSDs)," Proc. of the IEEE Intern. Symp. on Circuits and Systems, Vol. 6 , 31, May-June 1998, pp. 610-616.

[9] J.-A. Beraldin,"Design of Bessel-type Pre-Amplifiers for Lateral Effect Photodiodes," Int. J. Elec., 67, 1989, pp.591-615.

[10] J.-A. Beraldin, M. Rioux, F. Blais, L. Cournoyer, and J. Domey. "Registered intensity and range imaging at 10 mega-samples per second," Opt. Eng. 31(1), 1992, pp. 88-94.

[11] J.-A. Beraldin, F. Blais, M. Rioux, L. Cournoyer, D. Laurin, and S.G. MacLean, "Eye-safe digital 3D sensing for space applications," Opt. Eng. 39(1), 2000, pp. 196-211.

[12] T. Nezuka, M. Hoshino, M. Ikeda, and E. Asada. "A smart position sensor for 3-D measurement," Proceedings of the ASP-DAC 2001. Asia and South Pacific, 2001, pp. 21–22.

[13] F. Blais, M. Rioux, "Real-time numerical peak detector," *Signal Processing*, 11, 1986.

[14] D.K.Naidu, R.B. Fisher, "A comparative Analysis of Algorithms for Determining the Peak Position of a Stripe to Sub-pixel Accuracy," *Proc. British Machine Vision Conf.*, Glasgow, Scotland, 1991.

[15] G. Godin, J.-A. Beraldin, M. Rioux, M. Levoy, and L. Cournoyer. "An assessment of laser range measurement of marble surfaces," Proc. of the 5th Conf. on Optical 3-D Measurement Techniques, Vienna, Austria. October 1-4, 2001.

[16] N. Massari, L. Gonzo, M. Gottardi, A. Simoni, "High Speed Digital CMOS 2D Optical Position Sensitive Detector," in Proc. ESSCIRC, 2002, pp. 723-726.

[17] http://www.hamamatsu.com

[18] S. Ando and A. Kimachi. "A novel range finding system using correlation image sensor," Tech. Digest of the 17th Sensor Symp., Kawasaki, Japan, 2000, pp. 125-130.

[19] S. Yoshimura, T. Sugiyama, K. Yonemoto, and K. Ueda, "A 48kframe/s CMOS image sensor for real-time 3-D sensing and motion detection," in Digest of Technical Papers of 2001 IEEE International Solid-State Circuits Conference (ISSCC 2001), 2001, pp. 94–95.

[20] Y. Oike, M. Ikeda, and K. Asada. "Smart sensor architecture for real-time high-resolution range finding," in Proc. ESSCIRC, 2002, pp. 105-108.

[21] J.A. Cox. "Advantages of hexagonal detectors and variable focus for point-source sensors," Opt. Eng. 28(11), 1989, pp.1145-1150.

[22] B. F. Alexander and K.C. Ng. "Elimination of systematic error in subpixel accuracy centroid Estimation," Opt. Eng. 30(9), 1991, pp.1320-1331.